# The scale-dependence and structure of convergence fields preceding the initiation of deep convection

Cathryn E. Birch[1]*, John H. Marsham[2], Douglas J. Parker[2], Christopher M. Taylor[3]

[1]MetOffice@Leeds, University of Leeds, UK

[2]Institute for Climate and Atmospheric Science, School of Earth and Environment, University of Leeds, UK

[3]Centre for Ecology and Hydrology, Wallingford, UK

*Corresponding author: C. E. Birch, MetOffice@Leeds, School of Earth and Environment, University of Leeds, Woodhouse Lane, Leeds, LS2 9JT, UK. cathryn.birch@metoffice.gov.uk



This article has been accepted for publication and undergone full peer review but has not been through the copyediting, typesetting, pagination and proofreading process which may lead to differences between this version and the Version of Record. Please cite this article as doi: 10.1002/2014GL060493

**Abstract**

Links between convergence and convection are poor in global models and poor representation of convection is the source of many model biases in the tropics. State-of-the-art convection-permitting simulations allow us to analyse realistic convection statistically. Analysis of fractal dimension is used to show that in convection-permitting simulations (grid-spacings 1.5, 4 and 12km) of the West African monsoon 50% of deep convective initiations occur in the near vicinity of low-level boundary-layer convergence lines that are orientated along the mean wind. In these simulations more than 80% of initiations occur within large-scale (300 by 300km) convergence, with some 20% in large-scale divergence, and almost all cases occur within local-scale (60 by 60km) convergence. The behaviour alters in a simulation with a convection scheme and a grid-spacing of 12km; initiation is less frequent over convergence lines and there is less dependency on high-magnitude low-level local convergence.

## 1 Introduction

Representing the initiation and development of tropical convection in weather and climate models remains one of the key challenges in atmospheric science [*Stephens et al*., 2010]. Recent work using a high-resolution, convection-permitting modelling framework has explained how the inadequate representation of convection through parameterisation plays a significant role in continental-scale tropical biases [*Marsham et al*., 2013; *Birch et al*., 2014]. Tropical land areas provide a particular challenge because values of convective inhibition (CIN) can often be high, which means a dynamical forcing or "trigger" is generally required to bring parcels to their level of free convection and these triggers are generally not resolved in global models. Triggers may take the form of convergence lines, gravity waves, cold pool outflows, regions of elevated topography or surface 'hot-spots' from mesoscale variations in surface fluxes due to moisture availability and/or surface cover [*Pielke*, 2001].

Low-level convergence is a crucial part of the triggering process for multiple reasons. The associated lifting cools the mid-levels, thus increasing the Convective Available Potential Energy (CAPE) and reducing CIN, as well as increasing the relative humidity, which in turn reduces dry dilution through entrainment into convective plumes. On the cloud scale, lifting also provides a mechanism to overcome CIN, through the kinetic energy of ascending parcels. Reduced entrainment of dry air at convergence lines has also been shown to lead to increased humidity in the boundary layer, decreasing CIN [*Garcia-Carreras et al*., 2011]. *Birch et al.* [2013] present a case-study and show that the 100 km-scale low-level convergence is the first order determinant of whether or not a storm develops, although smaller scale processes determined the exact location and timing.

Most parameterisation schemes diagnose convection from the buoyancy, through a simple parcel ascent, and have no knowledge of the surrounding grid-boxes. Sensitivity experiments where various trigger functions have been tested within the same GCM show that the position, timing and intensity of convective activity vary substantially depending on the method employed [*Kain and Fritsch*, 1992] and can have major consequences for simulated convection and climate. This is especially true for the diurnal cycle of convection, where convection triggers almost immediately after sunrise over tropical land in many global models [*Bechtold et al.,* 2004]. *Birch et al.* [2014] show that the ability of models to trigger convection at the correct location and time is crucial for the regional water budget and thus the representation of the entire West African monsoon. Improving the triggering procedure to be more physically based has been shown to improve the diurnal cycle of tropical precipitation more widely [e.g. *Bechtold et al.*, 2004].

Our ability to run atmospheric models at higher resolution is increasing all the time. The UK Met Office has recently decreased the grid-spacing of its global operational numerical weather prediction model to 17 km in mid-latitudes. This resolution allows mesoscale structures to begin to be represented and is within the "grey-zone", where convection and mesoscale dynamics are partly resolved, while the statistical assumptions on which the parameterisation schemes are based do not hold. Within these developments lies a need and an opportunity to redesign convective parameterisation schemes to have a higher dependency on grid-spacing [*Arakawa et al.*, 2011] and to possibly make use of the mesoscale features that will be explicitly resolved. Certain information is required for these developments, such as the scale of convergence features that need to be captured in order to represent convective triggers and the statistics of convective activity in regard to larger-scale forcing.

In recent years we have, for the first time, gained the ability to run limited-area models with sub 5 km grid-spacing on continental-scale domains for periods of several months. This

development has, for the first time, provided an opportunity to analyse mesoscale features that have otherwise been extremely hard to observe in sufficient quantities to get good statistics, alongside large-scale fields such as convergence, which are very hard to observe with reasonable accuracy. *Taylor et al.* [2013] used this model framework to show that atmospheric models employing a conventional convective parameterisation scheme produce a precipitation-soil moisture feedback of the wrong sign, even at 12 km grid-spacing when the surface-driven mesoscale dynamics are reasonably well captured. On the other hand, running the same model at 12, 4 and 1.5 km grid-spacing with the convective parameterisation switched off produced a feedback of the opposite (and correct) sign, and the correct spatial structure. Similarly, an incorrect link between convergence and convection, will lead to errors in the diurnal cycle of convection, affecting energy budgets [*Parker et al.,* 2005], self-organisation of convection and coupled earth-system processes such as dust uplift [*Heinold et al*., 2013]. Since convective parameterisations are still undoubtedly needed at these resolutions, this suggests a need to develop schemes which are specifically designed for use on these grid-scales.

In this study convergence preceding the triggering of deep convection in model simulations with various horizontal grid-spacings is analysed statistically. First, a form of fractal dimension is used to illustrate the type and shape of mesoscale convergence features associated with convection initiation and their relationship with the mean wind. Second, the relationship between and relative importance of large-scale and local convergence are investigated. Within the analysis the dependency of these aspects on model grid-spacing and the way it represents convection are considered.

## 2 Model simulations and storm tracking

Met Office Unified Model (MetUM) limited-area model simulations were run over West Africa as part of the UK Cascade consortium project. The Cascade project uses large domain, free-running regional model simulations at a variety of horizontal grid-spacings to study convective organisation and understand model biases related to tropical convection. Simulations were performed with 12 km grid-spacing, employing the *Gregory and Rowntree* [1990] mass flux parameterisation (12P, *Walters et al.*, 2014), and with 12, 4 and 1.5 km grid-spacing (12E, 4E, 1.5E) where the convection scheme was switched off. The simulations were initialised with an ECMWF analysis at 0000 UTC, 26 July 2006. 12P, 12E and 4E were run for 40 days and 1.5E for 9 days. 12P and 12E were forced at the boundaries by ECMWF analyses every 6 h, 4E was forced at the boundaries by 12P every 30 min and 1.5E by 4E every 15 min. *Pearson et al.*, [2013] provide a more detailed description of the model configurations.

The initiation locations of storms are identified in the model simulations using a tracking algorithm developed by *Taylor et al.* [2011] for use with satellite observations and modified by *Taylor et al.* [2013] for use with these Cascade simulations. In summary, 15 minute precipitation totals from the simulations are used to identify contiguous rainy areas exceeding 1000 $km^2$ at any time of day. These features are then tracked back in time and space to the location and time of the first rainy grid cell. For 4E a total of 4320 initiations were identified over the 40 days (small black dots, Figure S1 in Supplementary material). In this study we focus on the Sahel domain highlighted in Figure S1, and exclude initiations where local topographic height exceeds 500m, resulting in a total of 1488 cases. Repeating this process using the 12P, 12E and 1.5E simulations gives 4051, 770 and 329 initiations respectively. Both 4E and 1.5E produce 37 initiations per model day and 12E produces 19. The difference is likely explained by the fact a grid-spacing of 12 km is coarse for a convection-permitting

simulation and only the strongest updrafts are able to cause sufficient uplift to initiate deep convection. Many more separate initiations are identified in 12P due to the showery rain it produces. For some aspects of the analysis only results from 4E are shown because the three configurations without convective parameterisation have a very similar statistical behaviour.

## 3 Analysis method and examples

For each simulation boundary-layer convergence is computed from the 925 hPa horizontal wind components at the initiation time (the results were found to be insensitive to the choice of convergence from this time or the preceding two hours). The area-mean convergence field, C, is analysed within squares centred over each of the initiation locations. The squares have sides of length L, where L varies from the size of the grid-spacing (e.g. 4 km in the case of 4E) to 300 km, to give convergence $C_4$ to $C_{300}$. The 'background' convergence field is also computed, by finding the mean convergence over the whole Sahelian sub-domain at all times.

We can understand the spatial distribution of convergence in terms of the magnitude of "local" convergence features, $C_{local}$ and the large-scale, background convergence, $C_\infty$, obtained when L becomes large. The examples in Figure 1 show two patterns of convergence from which convection is triggered:

1. Spatially distributed convergence (Figure 1a) where C is approximately constant, regardless of L:

$$C \sim C_\infty \sim C_{local}$$

2. Linear convergence (Figure 1b) where C decreases with L:

$$C \sim C_\infty + \frac{C_{local}}{L}$$

Similarly, we would expect an "isolated" convergence feature to display $C \sim C_{local}/L^2$. The shading in Figure 1c shows the contoured frequency of occurrence of C as a function of L based on 1488 events in 4E and suggests that C tends towards a large-scale limit at L>100 km and thus we assume $C_\infty \approx C_{300}$. The plot shows large variability in C on scales of L<36 km (vertical black line). This is the approximate accuracy limit of the algorithm, which is due to the hourly sampling of the winds (compared to 15 minutes for the precipitation), coupled to the transient or propagating nature of some of the convergence features.

We have chosen to analyse area-average convergence, C, because this is readily related to the mean vertical velocity on a given scale, through continuity. Assuming non-divergent flow, the mean upward velocities implied in Fig 2a at 1000 m altitude would be of the order 10 cm $s^{-1}$ for local convergence (360 m of ascent per hour) for local convergence and 1 cm $s^{-1}$ (~ 36 m $hr^{-1}$) for large-scale convergence. These figures tend to show that large-scale convergence is unlikely to be significant in triggering convection (although it can be significant in destabilising the profile) but local-scale convergent may trigger, or significantly erode CIN, over a few hours.

Taking into account the upper (L=100 km) and lower (L>36 km) lengthscale bounds discussed above the following analysis is performed on C between L=36 and 100 km, to compute a form of "mass-radius" fractal dimension [*Gouyet* 1996] for the convergence structures. For each initiation the 925 hPa convergence for each model grid square within the L=300km box is computed and $C_{300}$ is subtracted from each of them. We wish to compute logarithms of the function C(L), which cannot be done if C falls below zero for some L. Since at this stage only the shape of the convergence features is of interest, negative values of $C\text{-}C_{300}$ are set to zero and the mean is computed at each L (for the subsequent analysis in Section 5, the full field of C, retaining negative values, is used). For spatially-distributed convergence, $C\text{-}C_{300}$ is nearly constant with increasing L, while for linear features $C\text{-}C_{300}$

decreases with increasing L, as in the examples given above. Defining G to be the gradient of $\log(C\text{-}C_{300})$ against log(L) between L = 36 and 100 km, we can define a dimension, D, of the convergence pattern in each initiation case by:

$$D = G + 2 .$$

Localised features have a dimension, D, close to zero, linear features have a dimension close to 1, and features with spatially distributed convergence spread over an area have values of dimension close to 2. This is well illustrated by the two examples in Figure 1d; the gradient of example (a) (solid black line) between L = 36 and 100 km is -0.16, so that D=1.84 and the gradient of example (b) (dashed black line) is -0.95, so D=1.05. A number of initiations are associated with values of D>2, which represent cases where there are strong convergence features at larger distances away from the initiation point, so that the area-mean convergence increases with L.

**4 Shape and orientation of convergence features**

The shape of convergence features associated with initiations of deep convection is shown by the relative frequency of dimension, D, for each model configuration (Figure 2a). The median value of D for all three simulations where the convective parameterisation is not used is between 1.3 and 1.4, which suggests that more initiations occur due to one-dimensional (D=1) linear-shaped convergence patterns than for distributed (D=2) features. The median for 12P is 1.74, suggesting that 12P has more spatially distributed cases and fewer linear features. The differences between 12P and the simulations without convective parameterisation are not unexpected, since the trigger mechanism in the convective parameterisation in the MetUM does not have a convergence dependency and it is less able to form the organised mesoscale convective systems that occur in reality and that are reproduced by the explicit configurations (e.g. *Pearson et al.*, [2013]). There are almost no

instances of convective initiations over isolated features, for which D=0. Although a few isolated convergence features could be identified, these are typically weak, and the presence of larger convergence events in their neighbourhood tended to give D > 0.

The remainder of this section focuses on the orientation of convergence lines with respect to the mean wind, shown only for 4E. Initiations associated with linear features are identified using D = 1±0.4; 709 linear cases were identified out of a possible 1488 (48%), with similar results for 12E (51%) and 1.5E (46%) and a lower value of 27% for 12P. The lines produced by the model are similar in size and orientation to lines observed by radar near Niamey, Niger by *Dione et al.*, [2013] and in many cases appear to be related to areas of raised orography (not shown). The orientation of the convergence lines is derived from the L=300km convergence field; for each initiation all divergent parts of the field are set to zero and then the mean convergence is found for lines of every orientation between north-south to west-east, at an interval of 5°. The orientation of the convergence line is then identified by the rotated line with the largest mean convergence. Note that, for example, a west-east orientated line is equivalent to an east-west orientated line so the value of the orientation can only be between 180 and 360°. The orientation of the line in Figure 1b is identified as 240°, i.e. close to a southwest-northeast direction.

Figure 2b shows the relative frequency of the convergence-line orientations for 4E (solid line). The vast majority of cases involve convergence lines that are orientated in approximately a west-east direction (with variability between southwest-northeast and northwest-southeast, 225-315°). The mean wind directions are converted to a wind orientation for direct comparison with the line orientation (dashed line, Figure 2b) and the difference between the two angles is shown by the dot-dash line in Figure 2b, where negative (positive) differences represent cases where the wind is clockwise (anti-clockwise) of the convergence line. The majority of cases fall between -45 and +45°, illustrating that most of

the lines form along the mean wind, rather than perpendicular to it, and with no particular preference to be to the left or right of the wind at this level. The example in Figure 1b is representative of this; the southwest-northeast orientated convergence line forms in a mean southwesterly wind, immediately downstream of a region of elevated terrain with hill tops approximately 450 m above mean sea level (not shown). This result is consistent with Figure 1c in *Taylor et al*. [2013], who used the same 4E Cascade to show that the convergence associated with the storm initiations is on average linear and oriented along the mean wind.

**5 Large-scale convergence**

Many GCMs used for climate science currently have horizontal grid-spacings of order 100 km and thus cannot resolve convergence at the local ($C_{60}$ or less) scale. Convective parameterisation at these scales only has knowledge of the large-scale (gridbox average or aggregate) quantities. Although the current convective parameterisation in the MetUM does not have a convergence or vertical velocity dependency, other schemes, such as that by *Kain and Fritsch* [1993] do, which allows a more physical representation of convection [*Bechtold et al.*, 2004]. For future development it is necessary to know under what large-scale conditions convective storms are initiated. Figures 3a,b show the relative frequencies of C at the 300 and 60 km scales that are associated with initiations. For comparison, the background C is shown for 12P and 4E (12E and 1.5E have a very similar distribution to 4E). 12E, 4E and 1.5E have a similar distribution of $C_{300}$, with 83% of initiations occurring in large-scale convergence and 17% of cases occurring in large-scale divergence. The strong relationship between convective precipitation and convergence and the less frequent but relatively common occurrence of convective precipitation within large-scale divergence is consistent with the observational study by *Davies et al.*, [2013]. At the local scale convergence is much stronger in all three of the convection-permitting simulations (note

different axis scales in Figure 3a and 3b) and less than 10% of the initiations occur in divergence.

The relationship between initiation and large-scale convergence is different in 12P compared with the explicit run. Although a similar proportion of cases initiate in large-scale convergence (~80%), the magnitude of the convergence associated with the initiations is much weaker (Figure 3a). This is due in part to the weaker 12P background values (black dashed line), but also because the convection scheme does not respond to the convergence as the convection-permitting simulations do. The ratio of the pdfs of background $C_{300}$ convergence and $C_{300}$ for initiations is very different for parameterised and explicit, particularly for large values of convergence. The lack of response to the convergence is more apparent when comparing local-scale convergence ($C_{60}$, Figure 3b), where the tails of the 12E, 4E and 1.5E simulations extend to an order of magnitude greater than their background, whereas the tail of 12P only extends to twice the values its background.

In addition to the Cascade model simulations, the equivalent $C_{300}$ analysis was performed using observed initiations derived from satellite data by *Taylor et al.* [2011] and ERA-Interim winds (grey line Figure 3a) for June-September 2006. The line is centred almost exactly over $C_{300}$=0 $s^{-1}$, which illustrates that observed storms are not preferentially associated with large-scale convergence in ERA-Interim. There can be a number of explanations for this behaviour, including the failure of analyses to capture the convergence even on these scales (e.g. *Birch et al.* [2013]) and known biases in the location and diurnal cycle of ERA-Interim rainfall (common in GCMs, e.g. *Meynadier et al*. [2010]), and the results do suggest very strongly, in agreement with *Davies et al.* [2013], that large-scale convergence from a numerical weather prediction model should not be used as a predictive tool for tropical rainfall.

Figure 3c and d show large and local scale convergence from 4E split into day and night-time cases, along with the background values. At local scales ($C_{60}$) there is little dependency on time of day, indicating that the same magnitude of local convergence is associated with initiation of deep convection during the night and day. At large-scales ($C_{300}$) however, there is a much stronger diurnal dependency; at night the magnitude of both the background convergence and divergence is larger, which can be understood in terms of the tendency of synoptic and mesoscale circulations to intensify when the convective boundary layer mixing becomes small after sunset [*Parker et al*., 2005]. The ratio between the background and initiation lines is smaller during the day than at night, indicating that at night larger magnitudes of convergence are necessary to break through the stable nocturnal boundary layer.

## 6 Summary and conclusions

Where and when weather and climate models trigger deep convection is key for the correct representation of tropical convection and thus regional water cycles and monsoon circulations. Serious model biases originate from current methods of convective parameterisation [e.g. *Marsham et al*. 2013; *Birch et al.*, 2014]. This study uses large-domain, convection-permitting simulations at 1.5, 4 and 12 km grid-spacing to quantify the scales and structures of low-level mesoscale convergence contributing to the initiation of convection over West Africa in summer and to compare with a model simulation with parameterised convection. The large-domain, 40-day simulations allow a statistical analysis of more than 1000 storm initiations.

An analysis of the fractal dimension of convergence features is used to separate linear convergence features from other sources of convective initiation. The three convection-permitting simulations behave in a similar way; with 45-50% of initiations related to

convergence lines, similar in size and shape to those observed by *Dione et al.*, [2013], and the vast majority of the lines orientated along (within ±45° of) the mean wind, rather than perpendicular to it. In the convection-permitting simulations approximately 90% of cases occur within local convergence and more than 80% of the cases occur in large-scale convergence. At night convergence and divergence intensify as the flow responds to the reduction in drag from boundary-layer convection [*Parker et al.,* 2005] and convection is initiated in this convergence, which also likely sustains nocturnal convection [Crook and Moncrieff, 1988].

The simulation with the standard convection parameterisation shows different behaviour in the distribution of the fractal dimension of convergence, with fewer initiations at $D<1.5$ (34% in 12P, compared with 60% in 12E). Compared to the convection-permitting simulations, a similar fraction of the initiations occur in convergence/divergence but the magnitude of the convergence is much weaker in 12P and the parameterised convection responds differently to the convergence the model produces, being less responsive to strong convergence. This is perhaps not a surprise given that the convection parameterisation scheme in the MetUM has no explicit vertical velocity or convergence dependence.

Given the long-standing understanding of the relationship of convergence to convective initiation, these results do illustrate a fundamental problem in the way in which convective parameterisation schemes initiate convection. It is conceivable that this problem may be corrected by a better relationship between the thermodynamic profile (which is modified by large-scale convergence) and convection, but it is more likely that future parameterisations will have to take account of the convergence-triggering relationship in order to capture the location and timing of convection accurately in relation to larger-scale dynamics, and other parts of the climate system such as the land surface. Without improvement these errors will continue to cause major biases in the tropics. The Cascade simulations offer a framework to

evaluate the convergence-triggering relationships in different environments which can be used as a tool to evaluate the performance of convective parameterisations in future.

**Acknowledgements**

Access to the data sets used in this study is available from the corresponding author. The authors would like to thank Grenville Lister from Computer Modelling Support at National Centre for Atmospheric Science (NCAS-CMS) for running the simulations. This work made use of the facilities of HECToR, the UK's national high-performance computing service, which is provided by UoE HPCx Ltd at the University of Edinburgh, Cray Inc and NAG Ltd, and funded by the Office of Science and Technology through EPSRC's High End Computing Programme. The work undertaken by CEB is an output from a project funded by the UK Department for International Development (DFID) for the benefit of developing countries. The views expressed are not necessarily those of DFID. The work is based on results from the NERC-funded AMMA (NE/G018499/1) and Cascade projects (NE/E003826/1). The authors would like to thank Karsten Peters and Ben Shipway for their helpful comments. Thank you to Mitch Moncrieff and a second anonymous reviewer for their helpful comments.

**References**

Arakawa, A., J.-H. Jung, and C.-M. Wu (2011), Toward unification of the multiscale modelling of the atmosphere. *Atmos. Phys. Chem.*, 11, 3731-3742, doi:10.5194/acp-11-3731-2011.

Bechtold, P., J.-P. Chaboureau, A. Beljaars, A. K. Betts, M. Köhler, M. Miller, and J.-L. Redelsperger (2004), The simulation of the diurnal cycle of convective precipitation over land in a global model. *Q. J. R. Meteorol. Soc*., 130, 3119–3137, doi: 10.1256/qj.03.103.

Birch, C. E., D. J. Parker, A. O'Leary, J. H. Marsham, C. M. Taylor, P. P. Harris and G. M. S. Lister (2013), Impact of soil moisture and convectively generated waves on the initiation of a West African mesoscale convective system. *Q. J. R. Meteorol. Soc*., 139, 1712–1720, doi:10.1002/qj.2062.

Birch, C. E., D. J. Parker, J. H. Marsham, D. Copsey, and L. Garcia-Carreras (2014), A seamless assessment of the role of convection in the water cycle of the West African Monsoon, *J. Geophys. Res.*, DOI: 10.1002/2013JD020887.

Crook, N. A. and M. W. Moncrieff (1998), The effect of large-scale convergence on the generation and maintenance of deep moist convection, *J. Atmos. Sci*., 45, 3606-3624.

Davies, L., C. Jakob, P. May, V. V. Kumar, S. Xie (2013), Relationships between the large-scale atmosphere and the small-scale convective state for Darwin, Australia, *J. Geophys. Res.*, 118, 11534-11545, doi:10.1002/jgrd.50645.

Dione, C., M. Lothon, D. Badiane, B. Campistron, F. Couvreu, F. Guichard, S. M. Sall (2013), Phenomenology of Sahelian convection observed in Niamey during the early monsoon, *Q. J. R. Meteorol. Soc*., 140, 500-516, doi:10.1002/qj.2149.

Garcia-Carreras, L., D. J. Parker and J. H. Marsham (2011), What is the mechanism for the modification of convective cloud distributions by land surface-induced flows?, *J. Atmos. Sci*, 68, 619-634.

Gouyet, J.-F (1996), *Physics and fractal structures.* Masson, Paris. 234 pp. ISBN 2-225-85130-1.

Gregory, D., and P. R. Rowntree (1990), A mass flux convection scheme with representation of cloud ensemble characteristics and stability dependent closure, *Mon. Wea. Rev*., 118, 1483-1506.

Heinold, B., P. Knippertz, J. H. Marsham, S. Fiedler, N. S. Dixon, K. Schepanski, B. Laurent, and I. Tegen (2013), The role of deep convection and nocturnal low-level jets for dust emission in summertime West Africa: Estimates from convection-permitting simulations, *J. Geophys. Res.*, 118, 4385-440, doi:10.1002/jgrd.50402.

Kain, J. S., and J. M. Fritsch (1992), The role of convective "trigger function" in numerical forecasts of mesoscale convective systems, *Meteorol. Atmos. Phys*., 49, 93-106.

Kain, J. S., and J. M. Fritsch (1993), Convective parameterization for mesoscale models: The Kain-Fritsch scheme. The representation of cumulus convection in numerical models, K. A. Emanuel and D. J. Raymond, Eds., Amer. Meteor. Soc., 246 pp.

Marsham, J. H., N. Dixon, L. Garcia-Carreras, G. M. S. Lister, D. J. Parker, P. Knippertz, and C. E. Birch (2013), The role of moist convection in the West African monsoon system – insights from continental-scale convection-permitting simulations, *Geophys. Res. Lett*. 40, 1843-1849, DOI: 10.1002/grl.50347.

Meynadier, R., O. Bock, S. Gervois, F. Guichard, J.-L. Redelsperger, A. Agusti-Panareda, and A. Beljaars (2010), West African Monsoon water cycle: 2. Assessment of numerical weather prediction water budgets, *J. Geophys. Res*., 115, D19107, doi:10.1029/2010JD013919.

Parker, D. J., R. R. Burton, A. Diongue-Niang, R. J. Ellis, M. Felton, C. M. Taylor, C. D. Thorncroft, P. Bessemoulin and A. M. Tompkins (2005), The diurnal cycle of the West African monsoon circulation, *Q. J. R. Meteorol. Soc.*, 131, 2839-2860.

Pearson, K. J., G. M. S. Lister, C. E. Birch, R. P. Allan, R. J. Hogan, and S. J. Woolnough (2013), Modelling the diurnal cycle of tropical convection across the "Grey Zone", *Q. J. R. Meteorol. Soc.*, doi:10.1002/qj.2145.

Pielke, R. (2001), Influence of the spatial distribution of vegetation and soils on the prediction of cumulus convective rainfall, *Rev. Geophys.*, 39, 151-177.

Stephens, G. L., T. L'Ecuyer, R. Forbes, A. Gettlemen, J.-C. Golaz, A. Bodas-Salcedo, K. Suzuki, P. Gabriel, and J. Haynes (2010), Dreary state of precipitation in global models, *J. Geophys. Res.*, 115, doi:10.1029/2010JD014532.

Taylor, C. M., A. Gounou, F. Guichard, P. P. Harris, R. J. Ellis, F. Couvreux, and M. De Kauwe (2011), Frequency of Sahelian storm initiation enhanced over mesoscale soil-moisture patterns, Nat. Geosci., 4, 430–433, doi:10.1038/ngeo1173.

Taylor, C. M., C. E. Birch, D. J. Parker, N. Dixon, F. Guichard, G. Nikulin, and G. M. S. Lister (2013), Modeling soil moisture-precipitation feedback in the Sahel: Importance of spatial scale versus convective parameterisation, *Geophys. Res. Lett.*, 40, 6213-6218, doi: doi:10.1002/2013GL058511.

Walters, D. N. and coauthors (2014), The Met Office Model Global Atmosphere 4.0 and JULES Global Land 4.0 configurations, *Geosci. Model Dev.*, 7, 361-386, doi:10.5194/gmd-7-361-2014.

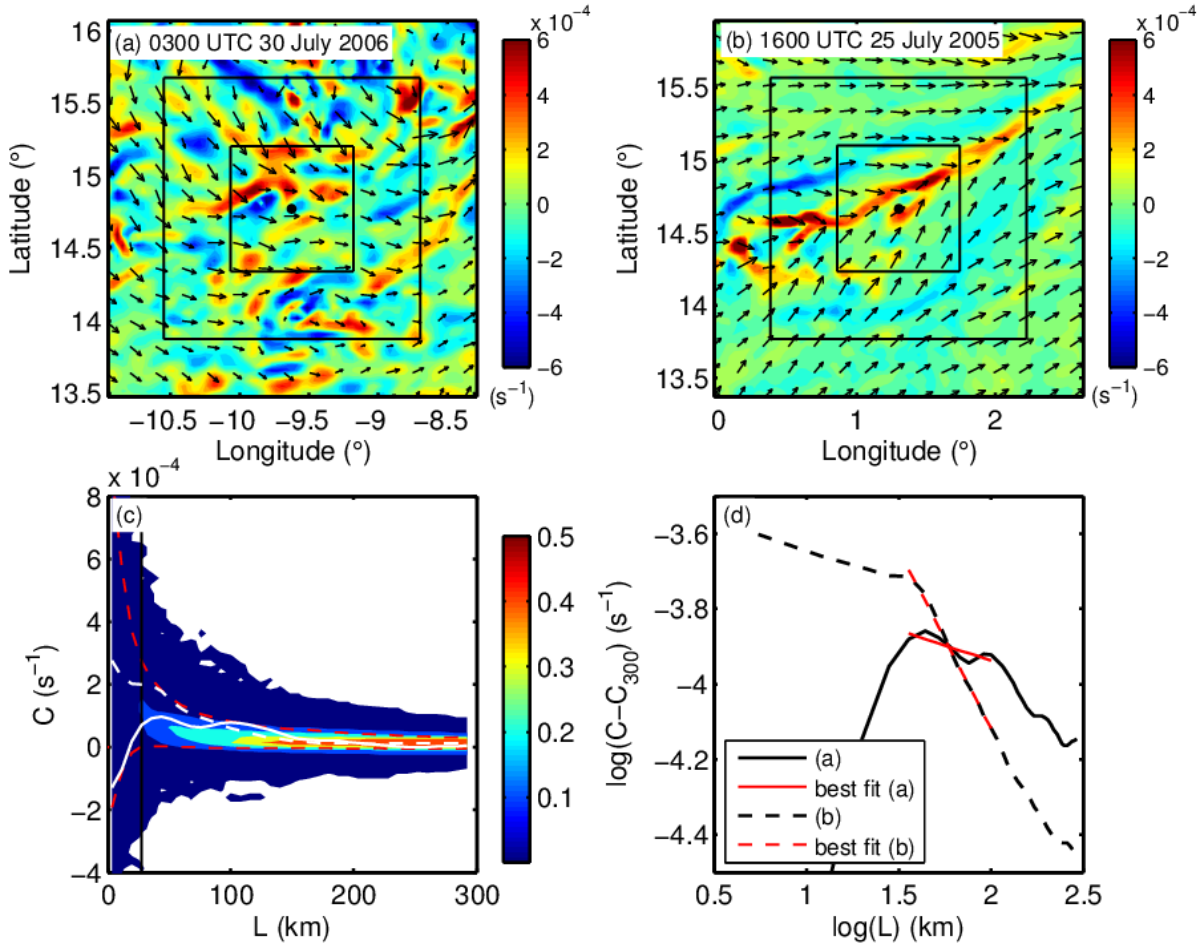


**Figure 1** Examples of (a) spatially distributed and (b) linear 925 hPa convergence features from 4E (shading). The arrows represent the horizontal wind at 925 hPa, the black dots the initiation location and the black squares boxes of L = 100 and L = 200 km. Shading in (c) shows the frequency of occurrence of mean C as a function of L, with 10$^{th}$ and 90$^{th}$ percentiles (red-dashed) for 4E. The solid and dashed white lines are for cases (a) and (b) respectively. (d) shows mean (C-$C_{300}$) as a function of L on logarithmic axes for the cases in (a) and (b). The red lines represent the lines of best fit in the range L = 36 to 100 km.

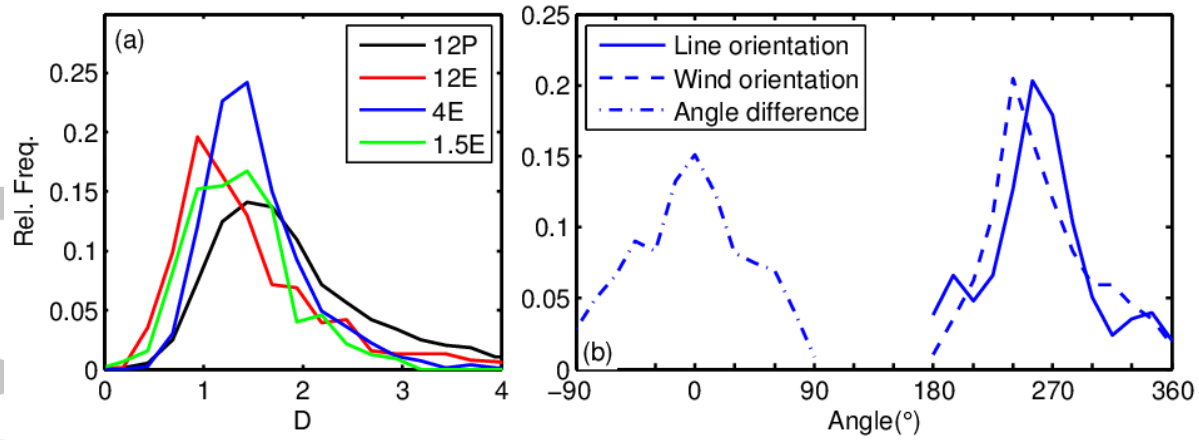


**Figure 2** Relative frequency of (a) dimension, D for each of the 4 model configurations, (b) the orientation of the mean wind for initiations associated with convergence lines (dashed line), the orientation of the convergence lines themselves (solid line), and the difference in angle between the two (dash-dot line). Negative differences mean the wind is clockwise of the line and positive differences mean the wind is anti-clockwise of the line. (b) is for 4E only.

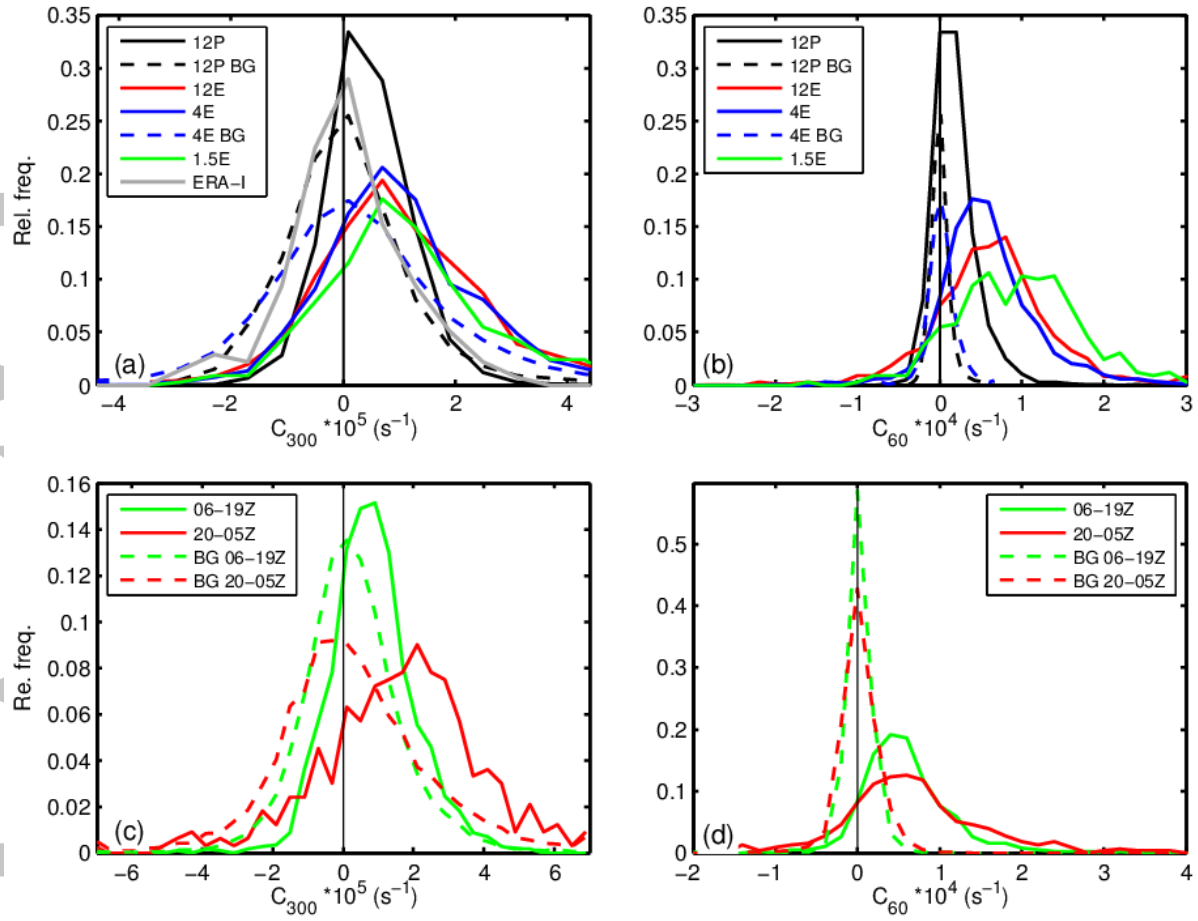


**Figure 3** (a) shows the relative frequency of large-scale convergence ($C_{300}$) for the four Cascade simulations (solid lines), the equivalent using initiations derived from satellite observations and ERA-Interim winds (grey solid line), and the background convergence for 12P and 4E (black and blue dashed lines). (b) is the same as (a) except for local-scale convergence ($C_{60}$). (c) and (d) show the relative frequency of $C_{300}$ and $C_{60}$ split by time of day for 4E.